2016 IEEE International Conference on Robotics and Automation (ICRA)
Stockholm, Sweden, May 16-21, 2016

SUAV:Q - A Hybrid Approach To Solar-Powered Flight

Ruben D'Sa, Devon Jenson, and Nikolaos Papanikolopoulos
dsaxx005@umn.edu, jens1172@umn.edu, npapas@cs.umn.edu
Department of Computer Science, University of Minnesota

***Abstract*— Selecting an aerial platform for an application typically requires compromise. A choice must be made between the flight time and long-range capabilities of a fixed-wing aircraft or the maneuverability and stationary characteristics of a multi-rotor platform. Recent developments of small-scale solar-powered UAVs have leveraged the advances in solar cell, energy storage, and propulsion system technology to reach extended flight times capable of all-day and multi-day flight.**

This paper presents the concept of a small-scale hybrid unmanned aerial vehicle capable of augmenting the maneuverability of a quad-rotor with the energy collection and supply of a solar-powered fixed-wing aircraft. An investigation into the aircraft design, transforming mechanism, and energy management of the multi-state system is presented.

A proof-of-concept prototype has been constructed to demonstrate the airframe operating in a quad-rotor configuration. Power electronics capable of simultaneous battery charging and power loading from a solar array have been validated. Additional work in optimization of the propulsion system and airframe needs to be completed to maximize the performance of the hybrid system.

I. INTRODUCTION

In recent years, aerial robotics has seen tremendous growth within the areas of both fixed-wing and multi-rotor flight. Although great achievements have been made in the domain of aircraft control, an area that has seen little development is that of solar-powered flight endurance and performance. Recently, a number of groups have shown development in the design of small-scale solar-powered aircraft [1], [2], [3]. Thanks to advancements in motor controller and motor performance, solar cell efficiency, and battery density, more solar energy can be captured and stored than what is required to fly at level flight. As a result, a number of these systems have demonstrated day-long and multi-day flight capability.

Several fixed-wing and flying wing systems have been capable of solar-powered flight [4], [5], [6]. To achieve a number of design goals, the size of these aircraft range between 4 meters [3], [7], [1] and 5.8 meters [2]. These systems have relatively high aspect ratio wings and, in order to meet the multi-day flight design goals, have correspondingly long wingspans. One of the greatest challenges with fixed-wing aircraft, compounded by a low Reynolds number and high aspect ratio wings, is maneuverability.

Multi-rotor systems are commonly used in applications that require both high maneuverability and the ability to hold a fixed spatial position. Their applications range from identification in search-and-rescue to characterization of nitrogen deficiencies in corn fields [8]. However, maneuverability and control come at the cost of high power consumption, resulting in short flight times. This is in contrast with the high efficiency, long-flight capable fixed-wing systems.

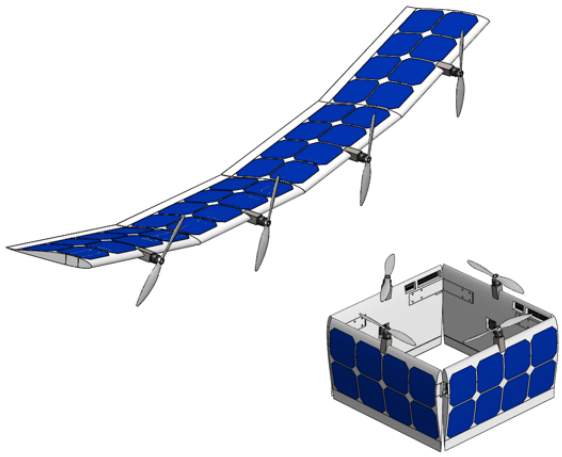

Fig. 1: Fixed-wing and quad-rotor states of the proposed SUAV:Q hybrid aircraft design.

As a solution to the restrictions faced when selecting either platform, this paper presents the design of a re-configurable solar UAV that is capable of transforming between fixed-wing and quad-rotor states. A platform capable of both states removes individual limitations and combines the strengths of both systems. In quad-rotor state, the aircraft cannot supply enough energy from solar power alone and will have to rely on stored energy. Once stored energy is close to being depleted, the aircraft will transition into a fixed-wing state where the on-board batteries will be able to recharge, allowing the process to repeat. A related approach to energy management has been applied to a solar-powered seaplane [9], where the ability to land on water enables long-term autonomous flight. Similarly, in this proposed design, vertical takeoff and landing allow the aircraft to wait on the ground for suitable solar conditions and land in the absence of them. By combining this functionality with a solar-powered system, the ability to achieve multi-day operation becomes feasible at very small scales. Traditionally, the size of solar-powered UAVs were limited due to energy storage requirements as the aircraft would have to store enough energy to supply power through the night. By relieving the constraint of carrying a large battery and replacing it with vertical takeoff and landing, the size of the aircraft can be dramatically reduced.

II. ROBOT DESIGN

This section discusses several important considerations in the design of the robotic aircraft: aircraft stability and weight

distribution, the mechanical transition between flight modes, and the transforming linkage design and analysis.

A. Approach

A number of propeller-based fixed-wing aircraft capable of vertical takeoff and landing have been developed. These systems range from very large-scale aircraft, such as the Boeing V22 Osprey, to very small-scale systems, such as the AeroVironment SkyTote [10]. In the case of the SkyTote, the design focused on high speed fixed-wing flight as opposed to the reduced energy consumption associated with low speed flight. While vertical take-off and landing sailplanes have been pursued [11], [12], this approach requires a large surface area while in a hovering state. Sailplanes also have limited hovering robustness due to their aircraft geometry. To develop a system that combines a high aspect ratio wing with the compactness of a quad-rotor, a sectioned reflexed chord plank wing is used. While control of a flying wing is more involved, the transformable design lends itself to a very stable quad-rotor design.

B. Aircraft Design

To facilitate the transitions between fixed-wing to quad-rotor states, a plank flying wing geometry was pursued. This design decision allows for motor and propulsion system assemblies to be mounted at the same longitudinal position, as opposed to a staggered arrangement. To provide roll stability, active hinges are used to transition the aircraft between wing states and are designed to have a hard stop that creates a built-in dihedral angle as shown in Figure 2.

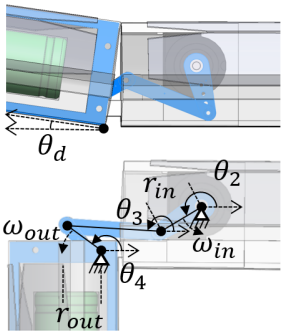

Fig. 2: Front view of the hinge section transitioning between fixed-wing and quad-rotor states. θ_d is the dihedral angle. ω_{in} and ω_{out} represent the input and output angular velocity respectively. r_{in} is the length of the servo arm and r_{out} is the length between the ground pivot and wing section weight vector which is assumed to be constant.

One of the challenges in designing aircraft with a flying wing geometry is lateral stability. In the selection of an aerofoil for a traditionally designed fixed-wing sailplane, the aircraft's tail elevator is used to counter the pitching moment of the main wing and center of gravity. In the case of a flying wing, no tail exists to counter this moment and both the aerofoil design and aircraft weight distribution must be selected accordingly. As discussed in [13], the elevator on a traditional aircraft can be designed into a single wing, resulting in a reflexed chord line aerofoil. By using a reflexed chord line aerofoil and adjusting the center of gravity of the aircraft to be in front of the neutral point (nose heavy), the reflexed tail section of the aerofoil will counter the pitching moment induced by the center of gravity and create a stable equilibrium point. The MH49 aerofoil was selected due to its performance at low speeds. Components were positioned to place the center of gravity in front of the neutral point as shown in Figure 3. A list of component weights are given in Table I. As the distance between the neutral point and center of gravity increases, the pitch stability increases, requiring a larger control surface. In order to minimize the area of the wing that is unable to be covered by solar cells, the center of gravity was adjusted to minimize the necessary control surface area while still providing adequate control authority.

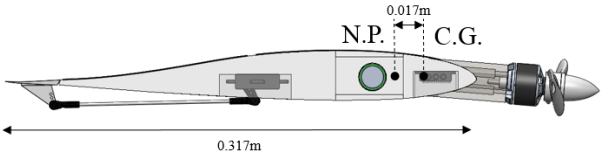

Fig. 3: Side view of the wing section illustrating the center of gravity (C.G.) and neutral point (N.P.) locations on a single wing section.

Component	Individual Section (g)	Entire System (g)
Solar Cells (8x SunPower C60)	108	430
Maximum Power Point Tracker	90	360
Battery Management System	31	124
Battery Mass (6x NCR18650B)	276	1104
Airframe	332	864
Propulsion System	94	376
Camera and Sensors	N.A.	0 to 300
Total	715	3364 to 3664

TABLE I: Estimated mass of the solar UAV prototype components.

In order to find the operating points that maximize energy performance of the aircraft, a vertex lattice method (VLM) analysis was performed using the software package XFLR5 [14]. An iterative approach was taken between adjusting component placement and the resulting global pitching moment. VLM analysis was performed using fixed lift polars with the lift equated to the mass of the aircraft. The results are shown in Figure 4. Using Figure 4(b), the optimum flight velocity for a system mass of 3.2kg is identified at 14.25m/s which can then be used to find the angle of attack in Figure 4(a).

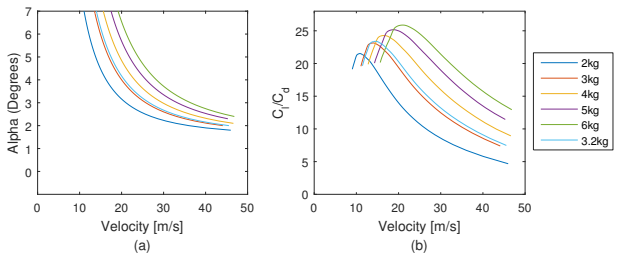

Fig. 4: Aircraft performance analysis using XFLR5 with VLM fixed lift polars equated to the mass of the aircraft. (a) Minimum angle of attack at a given velocity to ensure lift. (b) Ratio of coefficient of lift to coefficient of drag as a function of velocity. Maximum performance for a system mass of 3.2kg occurs at 14.25m/s with a C_l/C_d ratio of 23.40.

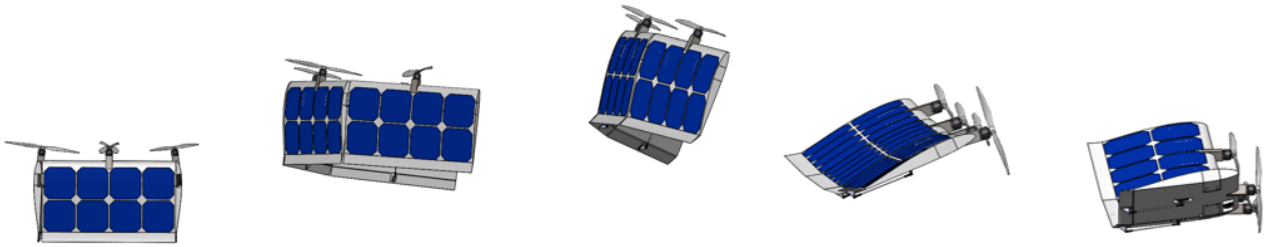

Fig. 5: Transition path from quad-rotor to fixed-wing states.

C. Forced State Transition

In order to minimize the size and mass of actuators used, the flight trajectory upon transition is selected to maneuver the aircraft into a state that minimizes the hinge actuation torque. By flying the aircraft in a near vertical state, the gravitational forces acting on the wing segments are oriented nearly parallel to the axis of hinge rotation, minimizing the torque required for actuation. A demonstration of this transition is shown in Figure 5. While transitioning from fixed-wing to quad-rotor state, the air resistance of the wing will resist transition. However, by minimizing the translational velocity of the aircraft, this force is reduced as shown in Figure 6. Currently, hinge operation is teleoperated and triggered by the flight controller. With additional modifications to flight controller firmware, on-board inertial measurement can be used as feedback to insure robustness of automated transitions. Management of the propulsion system torque in both states are shown in Figure 7.

D. Linkage Design

To provide actuation of the individual wing segments, a four-bar hinge mechanism is used. Shown in Figure 2 is the linkage in both fixed-wing and quad-rotor states. In order to minimize actuator energy power consumption in the fixed-wing state, the hinge enclosure has a built-in hard stop that limits the dihedral angle to the prescribed 8.7 degrees. A servo actuator was chosen over a linear actuator for its speed of actuation at the consequence of lower overall output torque. The 4-bar linkage was graphically synthesized and its mechanical advantage was evaluated using Equation (1) from [15] and plotted as a function of the angular position of the servo link in Figure 8. One of the mechanism design objectives was to build the system into the wing sections and minimize the gap surface between wing sections. This was achieved by anchoring the wing segment to the output link as opposed to the coupler link. Input no-load angular velocity is assumed to be a constant 428deg/s from a Power HD 1501MG with peak torque rated at 17kg·cm.

$$M.A. = \frac{r_{\text{in}}}{r_{\text{out}}} \frac{\omega_{\text{in}}}{\omega_{\text{out}}} \tag{1}$$

$$\omega_{\text{out}} = \frac{r_{\text{in}}}{r_{\text{out}}} \omega_{\text{in}} \frac{\sin(\theta_3 - \theta_2)}{\sin(\theta_3 - \theta_4)} \tag{2}$$

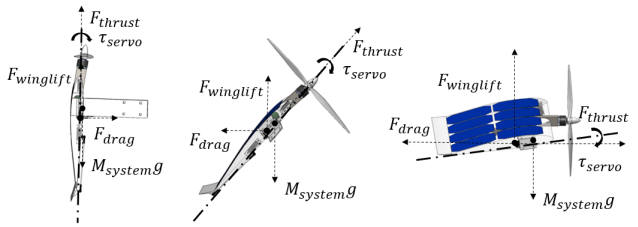

Fig. 6: Side view of forces and torques acting on the active hinge during transition between fixed-wing and quad-rotor states.

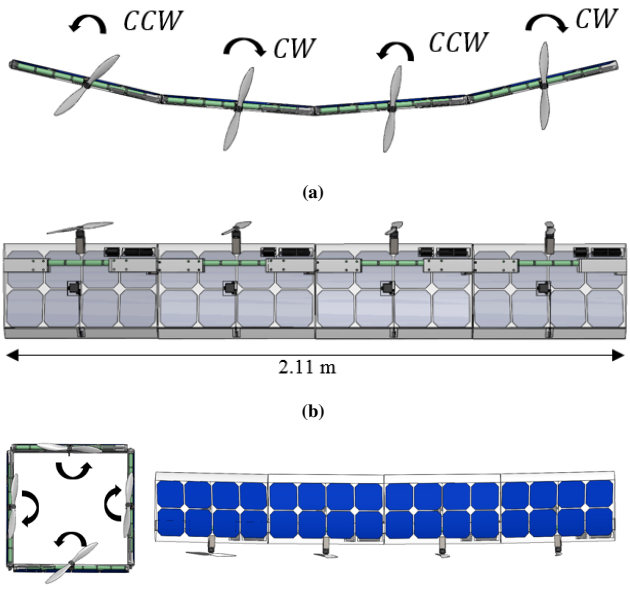

Fig. 7: (a) To manage the torque produced by each propeller and motor combination, the direction of rotation alternates such that the net induced torque by the propulsion system is balanced in both fixed-wing and quad-rotor configurations. (b) Each of the wing sections contain identical power electronics and battery hardware in order to manage the weight distribution across states. Shown in (c) is a comparison between the surface area difference between fixed-wing and quad rotor states.

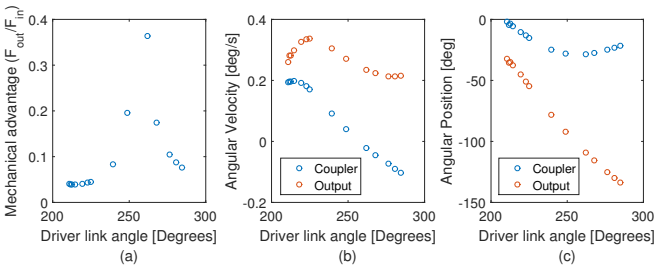

Fig. 8: Mechanical advantage and linkage angular velocity and position plotted as a function of driver link position.

III. Energy Framework

This section establishes a basic framework for evaluating the performance of a transformable solar-powered aircraft. A generalized system model is defined and used to analyze the performance of fixed-wing and rotor states for different battery sizes and payload. This analysis is concerned with hybrid operation of the aircraft, i.e. frequent transitions between fixed-wing and rotor states, and focuses on daytime flight where sufficient energy is available for rotor flight.

A. Hybrid System Model

The hybrid model consists of three states: fixed-wing, rotor, and ground. Fixed-wing and rotor states correspond to the right and left side of Figure 5. Their differences in lift generation provide a trade-off between power consumption and maneuverability. In ground state, the aircraft charges on the ground, typically in a fixed-wing orientation to maximize solar power intake. The following equations form the basis of the model. In level flight fixed-wing state, power consumption is given by [2] [7]

$$P_{\text{fixed}}(m_{\text{total}}) = \frac{P_{\text{level}}}{\eta_{\text{prop}}} = \frac{1}{\eta_{\text{prop}}} \cdot \frac{C_{\text{D}}}{C_{\text{L}}^{\frac{3}{2}}} \cdot \sqrt{\frac{2(m_{\text{total}} \cdot g)^3}{\rho \cdot A_{\text{wing}}}} \tag{3}$$

where η_{prop} is the propulsion system efficiency, C_{D} and C_{L} are the drag and lift coefficients that minimize level flight power, m_{total} is the total system mass (including energy storage and payload mass), g is the acceleration of gravity, ρ is the air density at a constant altitude, and A_{wing} is the wing reference area.

In rotor state, the power consumed during hover conditions is given by

$$P_{\text{rotor}}(m_{\text{total}}) = C_{\text{rotor}} \cdot {m_{\text{total}}}^{\frac{3}{2}} \tag{4}$$

where C_{rotor} is a constant defined for a particular rotor topology and m_{total} is the total system mass.

For solar power intake, the aircraft is assumed to be oriented with its wing segments open (as in fixed-wing state). This is shown in Figure 9.

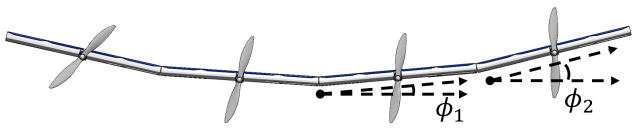

Fig. 9: Dihedral angles ϕ_1 and ϕ_2 of the SUAV:Q airframe in fixed wing state.

The solar power intake is given by

$$P_{\text{solar}}(t) = \max\left[0,\ I \cdot A_{\text{PV}} \cdot D \cdot \eta_{\text{PV}} \cdot \sin(\pi \cdot \frac{t}{t_{\text{day}}})\right] \tag{5}$$

$$D = \frac{\cos(\phi_1) + \cos(\phi_2)}{2} \tag{6}$$

where I is the peak solar irradiance, A_{PV} is the solar panel area, D is a constant that considers the angle of incidence due to the dihedrals, η_{PV} is the solar panel efficiency, and t_{day} is the length of day.

The available power in each of the three states is given by

$$P_{\text{avail, gnd}}(t) = P_{\text{solar}}(t) \tag{7}$$

$$P_{\text{avail, fixed}}(t) = P_{\text{solar}}(t) - P_{\text{fixed}}(m_{\text{total}}) \tag{8}$$

$$P_{\text{avail, rotor}}(t) = -P_{\text{rotor}}(m_{\text{total}}) \tag{9}$$

where it is assumed as a worst case analysis that no solar power is available in rotor state. Available power can be defined as the excess solar power in a given state. For it to be utilized, it must be able to be stored on-board for later use. In a deficit of solar power, power must be supplied from on-board storage to remain in the current state.

B. Power Levels and Energy Management

The three different states of the proposed hybrid vehicle provide different levels of available power. Energy can be managed by transitioning between these states to ensure a maximum use of available power and a minimum level of robustness. From an energy perspective, the aircraft moves between higher and lower energy states. For example, rotor flight can be thought of as a high energy state because it requires stored energy and can only be maintained for a relatively short period of time. Transitioning to a lower state (i.e., rotor to fixed-wing or rotor to ground) relaxes the energy required by the system.

Maximum use of available power is achieved by avoiding saturation of on-board energy storage. For hybrid aircraft, this means transitioning to rotor state before maximum capacity is reached. The battery's state of charge can also limit the charge rate and, as a result, limit the use of available power. It may be beneficial to set an upper energy threshold to ensure a minimum charge rate at all times.

A metric for robustness is stored on-board energy. In the event that available power is negative, due to flight power requirements or worsening solar conditions, stored energy can be used to transition to a lower state or maintain the current state. Similar to an upper threshold, the system can maintain a minimum amount of stored energy by transitioning to a lower state if the corresponding minimum energy threshold is reached. This guarantees a minimum level of robustness in all states, independent of the physical parameters of the system.

C. State Performance Parameters

An important parameter for hybrid aircraft is the charge or discharge time to a specified upper or lower threshold, $E_{\text{bat, thresh}}$, in a given state. This is given by the time t that solves the following equation

$$\int_{t_0}^{t} P_{\text{avail,state}}(t)\ dt + E_{\text{bat}}(t_0) = E_{\text{bat, thresh}} \tag{10}$$

As the fixed-wing state is used for both flight and intake of available energy, it has an associated charge time t_{fixed}. Rotor state requires stored energy and has an associated discharge

time t_{rotor} between thresholds. An upper threshold can be assigned as the energy required for an application specific rotor operation and, as described in the previous subsection, a lower threshold can be used to ensure a minimum level of robustness.

Because charge and discharge times depend on solar conditions and dynamic power consumption, a more general parameter is the ratio of time spent in a state,

$$t_{\text{ratio, state}} = \frac{t_{\text{state}}}{t_{\text{total}}} \tag{11}$$

where t_{total} is the total time spent in ground, fixed-wing, and rotor states.

A majority of hybrid operation occurs during the period when the fixed-wing state has available power (labeled t_{avail}). In this length of time, fixed-wing level flight is completely powered by solar and available power is stored for later use in rotor state. To optimize for both available energy and hybrid flight time, the aircraft should begin flight when P_{fixed} is first equivalent to P_{solar} (assuming on-board storage does not saturate before this time) and land after time t_{avail}. At the expense of stored energy, flight time can be extended before and after these points. These times and t_{avail} are given by,

$$t_{01} = \frac{t_{\text{day}}}{\pi} \arcsin\left(\frac{P_{\text{fixed}}}{I \cdot A_{\text{PV}} \cdot \eta_{\text{PV}}}\right) \tag{12}$$

$$t_{02} = t_{\text{day}} - 2t_{01} \tag{13}$$

$$t_{\text{avail}} = t_{02} - t_{01}. \tag{14}$$

D. Simulations - Battery Size and Payload

This subsection explores the effect of battery size and payload on state performance using the above system model. The conceptual design parameters used in the simulations are shown below in Table II. An estimate on the rotor constant, C_{rotor}, for the prototype design was determined empirically (see Section V).

η_{prop}	0.55
ρ	1.225 kg/m^3
A_{wing}	0.644 m^2
C_{rotor}	50.41 $W/kg^{3/2}$
I	1000 W/m^2
η_{PV}	0.22
A_{wing}	0.644 m^2
ϕ_1	8.7 degrees
ϕ_2	17.4 degrees

TABLE II: SUAV:Q conceptual design parameters used in simulations.

Fixed-wing performance is dependent on level flight power consumption. Figure 10 compares the available power and energy over the course of a 12-hour day with 30W and 60W fixed-wing flight powers. In each instance, the aircraft remains in ground state until P_{solar} is greater than P_{fixed} to optimize for both storage of available energy and flight time. It can be seen that as P_{fixed} increases, both $P_{\text{avail,fixed}}$ and t_{avail} decrease. This results in longer fixed-wing charge times and less overall available energy for larger payloads and batteries. If an upper energy threshold is required for rotor state operations, these operations will be less frequent. Figure 11 shows total available flight time (t_{avail}) and fixed-wing available energy ($E_{\text{avail, fixed}}$) as a function of total system mass. For each m_{total}, the coefficient of lift and the coefficient of drag that minimize level flight power were used. It can be seen that using a larger battery to increase robustness thresholds or extend flights beyond t_{avail} will degrade fixed-wing performance. Increasing battery size results in an approximately linear decrease in available energy.

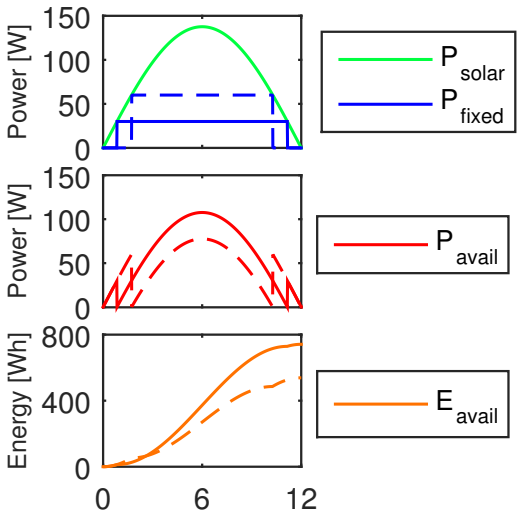

Fig. 10: Comparison of two different fixed-wing flight powers and their effects on available power and energy over the course of a 12-hour day; dashed lines represent 60W and solid lines represent 30W level flight powers.

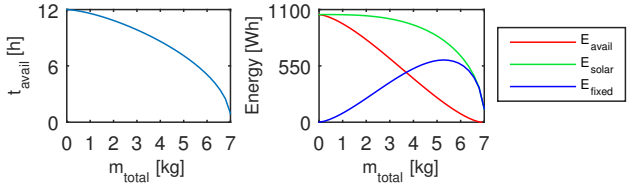

Fig. 11: Available flight time, solar energy, fixed-wing energy, and available energy as functions of total system mass.

Because rotor flight requires stored power, battery size is a critical parameter for rotor state performance. Figure 12 shows the effect of battery size on rotor flight time for various aircraft masses (i.e., mass of aircraft excluding battery mass). In this analysis, P_{rotor} was assumed constant. The transition between fixed-wing and rotor state is governed by the upper and lower energy storage thresholds. In this simulation the thresholds were set to the minimum and maximum energy capacity of the battery. For the simulated system mass and payloads, increasing battery size increases rotor flight time with diminishing returns. This means a small increase in rotor flight time requires a longer fixed-wing charge time. In other words, the proportion of total flight in rotor state becomes smaller with increasing battery size. Figure 13 shows the state of each aircraft from Figure 12, at the operating point of twelve battery cells, over the course of a 12-hour day. It can be seen that increasing m_{aircraft} for a

given battery size decreases t_{total}, $t_{\text{ratio, rotor}}$, and t_{rotor}. For best performance, the battery should be sized for the maximum m_{aircraft} and t_{rotor} required by a specific application.

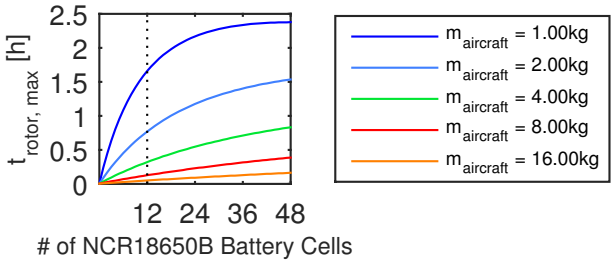

Fig. 12: Rotor flight time (t_{rotor}) as a function of NCR18650B battery cells (interpolated between discrete points); $m_{\text{total}} = m_{\text{aircraft}} + m_{\text{battery}}$.

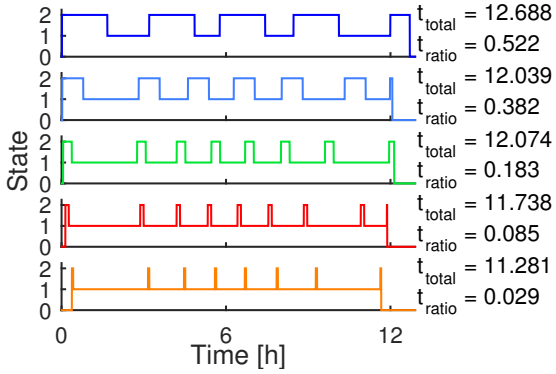

Fig. 13: Aircraft state (0 = ground, 1 = fixed-wing, 2 = rotor) over a 12-hour day with 12 NCR18650B cells and various aircraft masses. The aircraft masses follow the legend of Figure 12. t_{ratio} is the ratio of total flight time (t_{total}) spent in rotor state. For each aircraft, once the corresponding t_{02} was reached, the aircraft transitioned to rotor state until the remaining stored energy was depleted.

IV. Electrical Hardware

Figure 14 is an illustration of the hardware topology of the SUAV:Q. Each of the four wing sections contain an identical configuration of power electronics and batteries. Within each wing segment, the placement of components is such that the center of gravity lies at the longitudinal mid-section. The intent of even weight distribution is to maximize stability in both quad-rotor and fixed-wing states.

Each wing section contains 8x SunPower C60 solar cells capable of 24 watts. In fixed-wing configuration and with ideal solar conditions, the power system is capable of supplying 96 watts from the solar array. Due to the I-V characteristics of solar cells, the impedance of the load must be closely matched with the output impedance of the solar array. Given the varied angle of solar irradiance hitting each angled section of the aircraft, each section requires a maximum power point tracker (MPPT). Each MPPT is used to track and adjust the voltage operating point of its corresponding panel to ultimately maximize the amount of solar power available to the aircraft. In addition to the MPPT, each of the lithium ion cells is monitored by a battery protection system to protect against over-voltage and unbalanced cells.

Power is monitored throughout the system using the TI INA219 current shunt and power monitor. Each module communicates with an ATmega328 over an I2C bus. Voltage and current measurements received by the ATmega328 are stored locally to an SD card as well as relayed in real-time using 915MHz radios to a ground station.

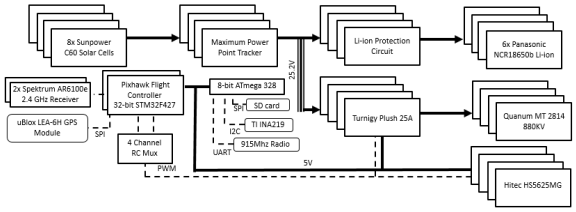

Fig. 14: Electrical power and communication topology for the SUAV:Q. Identical batteries, power conversion, speed controllers, and actuation servos are used across all four segments.

To control the aircarft, two Pixhawk autopilots are used. A 4-channel PWM multiplexer is used to switch throttle control of the four electronic speed controllers between the two flight controllers, where one is configured for fixed-wing and the other quad-rotor flight. Teleoperation of the system is performed using a Spektrum DSMX transmitter and receiver combination. Using an external u-blox LEA-6H GPS module, the system can be set to fly to prescribed GPS way points. A single PWM signal is used to control all four hinge servos and is configured in the Pixhawk to be remotely controlled by a toggle switch on a Spektrum DX8 transmitter.

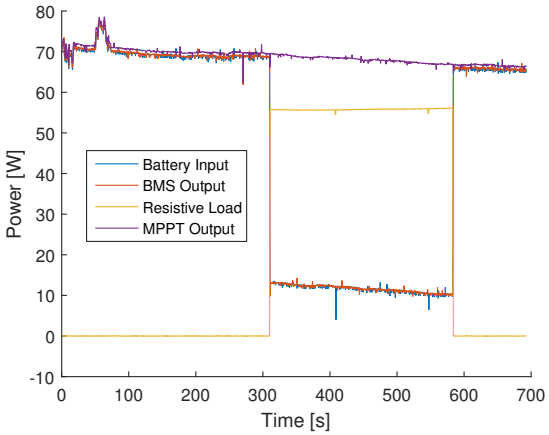

Fig. 15: Solar power system charging 36 Panasonic NCR18650b cells connected in a 6s6p configuration. A 10ohm resistive load was connected to the output to represent power draw from the SUAV:Q propulsion system. Initial peak in solar power was due to array alignment with respect to the sun. Average collected solar power was 68.92W. Test data was collected on Sept. 13, 2015 at Nils Hasslemo Hall, Minneapolis, MN at 5:45pm.

V. Experimental Tests

Figure 15 shows the results from an outdoor test of 32 SunPower C60 cells along with a 6s battery management system and 36 Panasonic NCR18650B cells wired in a 6s6p configuration. An LT8490 based MPPT was connected between the solar cells and the battery. The battery cells were protected by a PCM-LI22.2V20A battery management system for 6s battery configurations. In order to simulate a step

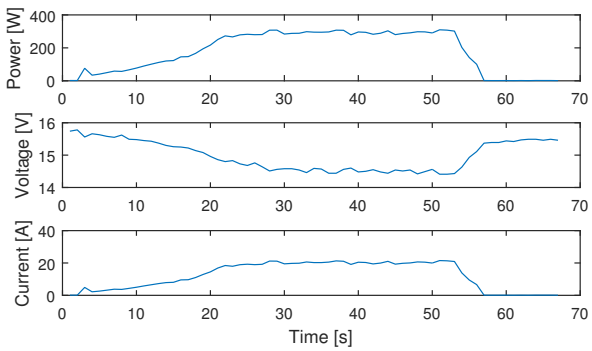

Fig. 16: Battery voltage, current, and power draw from the prototype airframe operating in the quad rotor configuration. Average power consumption during hover was measured at 288.57W with a 4s1p 4000mAh LiPo configuration and a system mass of 3.2kg. Test data was collected in-doors with minimal wind disturbance.

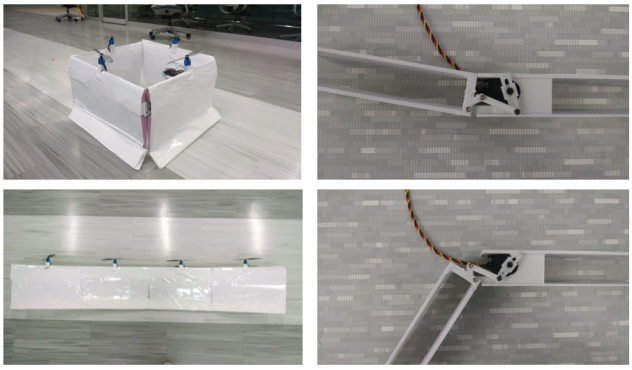

Fig. 17: Prototype system airframe in both fixed wing and quad rotor configurations. Active hinges were fabricated using an FDM 3D printer and PLA filiment.

load response, a 10Ω 200W power resistor was connected in parallel with the MPPT output. Upon connecting the resistive load, the MPPT output stayed constant, reducing the battery charging power level to satisfy the load requirements as expected. Power consumption data and photos of the prototype in quad-rotor configuration are shown in Figure 16 and Figure 17.

VI. Conclusions and Future Work

Presented in this paper are the aircraft design and energy framework for a hybrid quad-rotor to solar-powered fixed-wing UAV. Lift characteristics of the aircraft design were simulated and optimum operating conditions were determined. Performance of the active hinge was evaluated using techniques from linkage analysis. Models for the operating time across the multi-state system were parameterized to take into account temporal changes in solar irradiance and system mass, illustrating the flexibility of the hybrid system to maximize use of available energy. Power system electronics were validated using 32 SunPower C60 cells and functionality in the quad-rotor state was demonstrated.

Work is underway to improve the current prototype, most notably in the areas of washout aerofoil design and optimal control surface sizing. Validation of prototype operation in fixed-wing and transition between states needs to be performed. Improvements to the propulsion system will need to be made; the propeller and motor combination will need to be sized to a dynamic thrust rather than a static thrust to minimize level flight power consumption. The general energy model is currently being expanded to include state transition energy and a detailed propeller-motor analysis for fixed-wing and rotor states.

VII. Acknowledgements

This material is based upon work supported by the National Science Foundation through grants IIP-0934327, IIS-1017344, IIP-1332133, IIS-1427014, IIP-1432957, OISE-1551059, CNS-1514626, CNS-1531330, and CNS-1544887. Ruben D'Sa was supported by a National Science Foundation Graduate Research Fellowship No. 00039202.

References

[1] A. Noth, W. Engel, and R. Siegwart, "Design of an ultra-lightweight autonomous solar airplane for continuous flight," *Field and Service Robotics*, vol. 25, pp. 441–452, 2006.

[2] P. Oettershagen, A. Melzer, T. Mantel, K. Rudin, R. Lotz, D. Siebenmann, S. Leutenegger, K. Alexis, and R. Siegwart, "A solar-powered hand-launchable uav for low-altitude multi-day continuous flight," in *IEEE International Conference on Robotics and Automation (ICRA)*, May 2015, pp. 3986–3993.

[3] S. Morton, R. D'Sa, and N. Papanikolopoulos, "Solar powered uav: Design and experiments," *IEEE/RSJ International Conference on Intelligent Robots and Systems (IROS), Hamburg*, vol. 14, no. 1, pp. 2460–2466, 2015.

[4] T. Noll, J. Brown, M. Perez-Davis, S. Ishmael, G. Tiffany, and M. Gaier, "Investigation of the Helios prototype aircraft mishap report, NASA," 2004.

[5] J. Amos, "'Eternal plane' returns to Earth. BBC News, 2010. "http://www.bbc.co.uk/news/science-environment-10733998."

[6] K. Flittie and B. Curtin, "Pathfinder solar-powered aircraft flight performance," vol. 4446. AIAA, 1998.

[7] S. Morton, L. Scharber, and N. Papanikolopoulos, "Solar powered unmanned aerial vehicle for continuous flight: Conceptual overview and optimization," in *IEEE International Conference on Robotics and Automation (ICRA)*, 2013, pp. 766–771.

[8] D. Zermas, D. Teng, P. Stanitsas, M. Bazakos, V. Morellas, D. Mulla, and N. Papanikolopoulos, "Automation solutions for the evaluation of plant health in corn fields," *IEEE/RSJ International Conference on Intelligent Robots and Systems (IROS), Hamburg*, 2015.

[9] R. D. Eubank, "Autonomous flight, fault, and energy management of the flying fish solar-powered seaplane." Ph.D. dissertation, University of Michigan, 2012.

[10] A. Koehl, H. Rafaralahy, M. Boutayeb, and B. Martinez, "Aerodynamic modelling and experimental identification of a coaxial-rotor uav," *Journal of Intelligent and Robotic Systems*, vol. 68, no. 1, pp. 53–68, 2012.

[11] S. Verling and J. Zilly, "Modeling and control of a VTOL glider," Bachelor Thesis, Autonomous Systems Lab, ETH Zurich, April 2013.

[12] T. Matsumoto, K. Kita, R. Suzuki, A. Oosedo, K. Go, Y. Hoshino, A. Konno, and M. Uchiyama, "A hovering control strategy for a tail-sitter vtol uav that increases stability against large disturbance," in *IEEE International Conference on Robotics and Automation (ICRA)*, May 2010, pp. 54–59.

[13] M. Hepperle, "Design of flying wing models," http://www.mh-aerotools.de/airfoils/flywing1.htm, 2015.

[14] A. Deperrois, "Stability analysis using XFLR5," http://www.xflr5.com/docs/XFLR5_and_Stability_analysis.pdf, 2010.

[15] A. Erdman, *Mechanism Design: Analysis and Synthesis*. Upper Saddle River, NJ: Prentice Hall, 2001.